JOURNAL OF PROPULSION AND POWER
Vol. 23, No. 5, September–October 2007

Mach-8 Tests of a Combined-Cycle Engine Combustor

Kanenori Kato,* Takeshi Kanda,† Kenji Kudo,‡ and Atsuo Murakami
Japan Aerospace Exploration Agency, Miyagi 981-1525, Japan

DOI: 10.2514/1.29018

Under the Mach-8 flight condition, combined-cycle-engine combustor tests were conducted. The combustor model had a two-rocket fuel injector, which supplied fuel-rich, precombustion gas as fuel. Gaseous hydrogen and oxygen were used as propellants. Two combustion patterns were observed for various lengths of the straight duct connected to the rocket injector section. In the longer straight-duct configurations, combustion gas was decelerated to subsonic speed and choked thermally at the exit of the straight duct. In the shorter straight-duct configurations, combustion progressed in the downstream divergent duct. Pitot pressure and gas-sampling parameters were measured at the exit plane of the combustor model. Results showed that a certain length of a constant cross-sectional area combustor section was required to sustain combustion of the rocket plume injected parallel to the airflow.

Nomenclature

A	=	cross section
H	=	height of the straight-duct section
L	=	length of the straight-duct section (including the straight part of the combustor downstream of the rockets)
$\dot{m}$	=	mass flow rate
$(O/F)_r$	=	mass flow ratio of oxygen to fuel in the rocket
P_w	=	wall pressure
P_{wi}	=	wall pressure at the entrance of the combustor
R_0	=	universal gas constant
T_t	=	total temperature of inflow air
W	=	molecular weight
x	=	distance from the exit of the rocket nozzle
y	=	spanwise distance from the sidewall surface
z	=	distance from the rocket sidewall
γ	=	ratio of specific heat
η_c	=	combustion efficiency
ϕ	=	equivalence ratio

I. Introduction

STUDIES of a space plane are being carried out to create a new transportation system for use to and from low Earth orbit. Although the scramjet engine shows high performance when used in a single-stage-to-orbit (SSTO) space plane, other engines are necessary for the SSTO plane to cover all of the speed regions and attain low Earth orbit. When several engines are mounted on a vehicle, the propulsion system becomes a combined system, therefore, combined-cycle engines for the space plane have been studied [1–3]. The Japan Aerospace Exploration Agency (JAXA) has been studying the rocket–ramjet combined-cycle engine. This engine has rocket engines in the combustor and its operation consists of an ejector-jet mode, a ramjet mode, a scramjet mode, and a rocket mode. This engine will be used not only for the SSTO space plane, but also for atmospheric hypersonic vehicles. In the present study, combustion tests with a combined-cycle-engine combustor model, which was designed based on a conceptual study [3], were conducted. This combustor model had two rockets in the combustor section, which were used not only for thrust production, but also for the fuel supply for secondary combustion.

In the scramjet mode, the fuel was applied in the hydrogen-rich rocket exhaust, which flowed parallel to the breathed supersonic airflow. With parallel fuel injection, sufficient mixing and reaction are key factors in the performance of the scramjet. Because the configuration of the fuel injector in the scramjet mode is different from that of the conventional scramjet engine type that has been tested at JAXA, mixing and reaction techniques are more vital subjects in the scramjet mode of the combined-cycle engine. Therefore, reasonable operation of the engine under the Mach-8 flight condition should be demonstrated, and its characteristics and problems must be clarified to enable development of a combined-cycle engine. Combustion tests were conducted to investigate whether high performance could be attained by parallel fuel injection from precombustion rocket exhaust. The L/H effect of the straight duct downstream of the rockets was also investigated. A divergent-duct extension was also included.

II. Experimental Facility

Figure 1 shows a schematic illustration of the combustor model (measurement in millimeters). The combined-cycle-engine combustor model was directly connected to a hot-gas generator [4]. The thrust force was not directly measured by a force measurement system. The airflow was heated in a hydrogen vitiation heater and accelerated to Mach 2.4 through a supersonic nozzle. The airflow first entered an isolator with a constant cross-sectional area and a length of 100 mm. The cross-sectional area of the rocket section entrance was 32 mm wide and 147.3 mm high. There were two rockets in the rocket section. The throat diameter and exit diameter of the rocket were 9.2 and 14.0 mm, respectively. Gaseous hydrogen and gas oxygen at room temperature were supplied to the rockets as propellant; the ratio of the mass flow rate of oxygen to fuel in the rocket, $(O/F)_r$, was 0.5 in this study. Because the operation of the engine in this study was mainly for supersonic transportation, such a low mixture ratio was selected in the conceptual study [3] to maintain thrust production by the rockets and prevent significant degradation of overall specific impulse. The c^* efficiency of the rockets was 0.95, and the combustion efficiency was 0.88, according to the measured pressure in the rocket chambers. The rocket chamber pressure was measured directly with two mechanical scanners (Scanivalve®). The Mach number at the exit of the rocket was 2.2. The equivalence ratio was defined with the remaining hydrogen within the rocket plume with respect to the incoming flow from the facility nozzle. To guide the airflow to the rocket side of the combustor, a ramp block was installed between the rockets and between the rockets and sidewalls. The angle of the ramp was 11.3 deg.

Received 27 November 2006; revision received 9 April 2007; accepted for publication 16 April 2007.

*Senior Researcher, Combined Propulsion Research Group, Space Propulsion Center 1 Koganezawa, Kimigaya, Kakuda. Member AIAA.

†Director, Combined Propulsion Research Group, Space Propulsion Center 1 Koganezawa, Kimigaya, Kakuda. Senior Member AIAA.

‡Senior Researcher, Combined Propulsion Research Group, Space Propulsion Center 1 Koganezawa, Kimigaya, Kakuda.

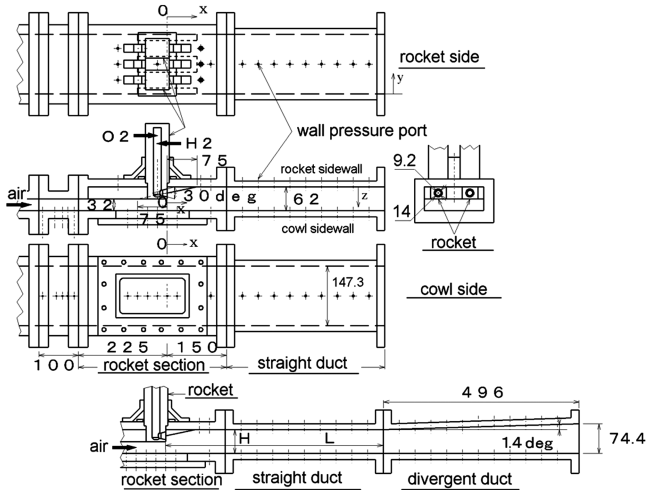

Fig. 1 Schematic illustration of the combustor model.

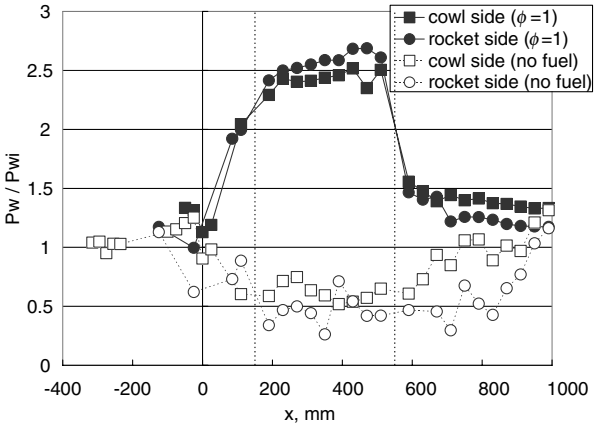

Fig. 2 Wall pressure distribution with 400-mm straight duct.

There was a straight-duct section downstream of the rocket section. In this study, four kinds of straight ducts were used to investigate the effect of the length of the straight-duct section. The lengths of these ducts were 160, 240, 320, and 400 mm. The cross section of the straight duct was 62 by 147.3 mm. There was a divergent-duct section downstream of the straight-duct section with a 1.4-deg divergent angle at the rocket side. The length of the divergent duct was 496 mm and the cross section of its exit was 74.4 by 147.3 mm.

High-enthalpy airflow was created by the hydrogen–oxygen–air vitiation heater. The total pressure and the total temperature of the air were 1.05 ± 0.05 MPa and 2400 ± 50 K, respectively. The mole fraction of the unreacted oxygen in the heated air was $21 \pm 1\%$. These airflow conditions simulated the enthalpy level of flight condition at Mach 8.

The x axis was in the direction of the airflow and its origin was at the exit of the rocket nozzle position. The y axis was in the lateral direction and its origin was on the sidewall. The z axis was in the longitudinal direction and its origin was on the rocket sidewall.

Pressure taps were aligned on the centerline of both walls (cowl side and rocket side). Wall pressure was measured with two mechanical scanners (Scanivalve) in the 30-ms sampling period. The accuracy of pressure was ± 1.4 kPa in the wall and pitot pressure. The pitot pressure measurement and gas sampling were conducted at the exit of the straight duct and at the exit of the divergent duct to estimate mean properties of the combustion gas [5]. A water-cooled pitot rake was used. Measurements were performed at 60 locations (6 in the z direction by 10 in the y direction) in each plane. Sampled gas was analyzed by gas chromatography (Micro-GC VP2000®). The nearest wall pressure was substituted for the static pressure to calculate the gas properties with the measured pitot pressure. The error bars for the equivalence ratio, combustion efficiency, and Mach number were ± 1, ± 1, and $\pm 7\%$, respectively.

III. Results and Discussion

A. Long Straight-Duct Configuration

Figure 2 shows the wall pressure distributions at $T_t = 2400$ K, $(O/F)_r = 0.5$, and $\phi = 1.0$ in the case of the 400-mm straight-duct configuration.

The vertical broken lines indicate the positions of the entrance and exit of the straight duct. The pressure under no-rocket-exhaust conditions (i.e., no fueled conditions) is also plotted. The pressure was normalized with the wall pressure at the entrance of the isolator (i.e., at the exit of the facility nozzle). The wall pressure at the entrance of the isolator was 65 ± 1 kPa. The ambient pressure (1 atm) is 1.54 in the figure.

The wall pressure increased in the straight-duct section. It was 2.5 times higher than that of the inflow air. The wall pressure was not high around the exit of the rocket nozzle. It increased downstream of the rocket nozzle and decreased slightly toward the exit of the straight-duct section. The wall pressures on both sides were almost identical. This feature indicated that the combustion gas was in the subsonic condition in the straight duct.

The choked pressure was calculated as follows at the $M = 1$ condition:

$$P = \frac{\dot{m}}{A}\sqrt{\frac{R_0 \cdot T_t}{\gamma \cdot W}}\sqrt{\frac{2}{\gamma + 1}} \tag{1}$$

In this case, $T_t = 3090$ K, $\gamma = 1.19$, and $W = 20.3$. The estimated choked pressure was 140 kPa. The choking condition became $P_w/P_{wi} = 2.1$, which was in agreement with the experimental results. This also means that combustion gas was in the subsonic condition in the straight-duct section. The combustion gas became subsonic and choked thermally at the exit of the straight duct. Though the pressure at the exit of the divergent duct was lower than the ambient pressure, measurement toward the exit showed no increase of pressure. This indicated that no separation was formed under this combustion condition.

Figures 3a–3c show the distributions of the local equivalence ratio, the local combustion efficiency, and the Mach number at the exit of the straight duct, respectively. Mean properties are listed in Table 1.

The broken lines indicate the positions of rockets. These results were obtained based on the measured pitot pressure and the sampled gas analyzed by gas chromatography. The equivalence ratio was larger on the rocket side. The combustion efficiency was distributed around 0.8 to 0.9 on most of the measured plane. There was a subsonic region on the rocket side. Though there was a supersonic region on the cowl side, the mean velocity of the combustion gas was subsonic.

To examine the combustion conditions at the exit of the straight duct, probing was also conducted. Figures 4a–4c show the distributions of the local equivalence ratio, the local combustion efficiency, and the Mach number at the exit of the divergent duct, respectively.

At the exit of the divergent duct, the mean velocity became supersonic. The combustion gases that choked at the exit of the straight duct were accelerated in the divergent duct and became supersonic. The Mach number and equivalence ratio were distributed more uniformly than those at the exit of the straight duct.

Table 1 Combustion gas properties in the case of the 400-mm straight duct

Position	η_c	M	Impulse function
Straight duct exit	0.74	0.79	2270 N
Divergent duct exit	0.82	1.30	2693 N

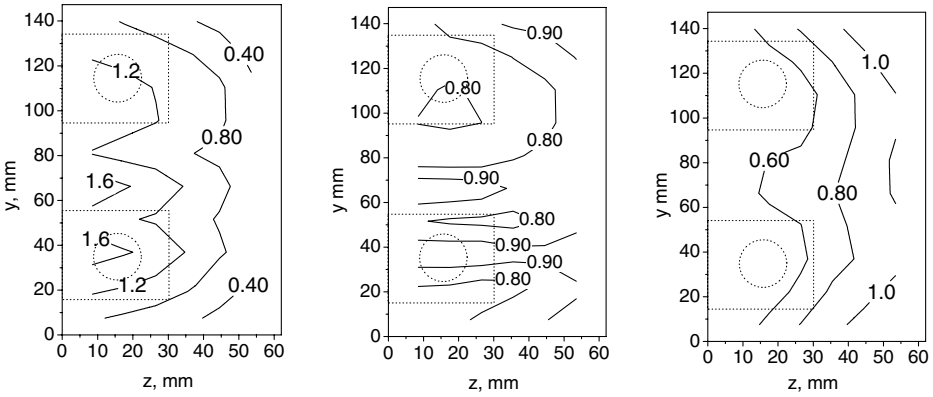

a) Equivalence ratio b) Combustion efficiency c) Mach number

Fig. 3 Properties of combustion gas at the exit of the straight duct in the case of the 400-mm straight-duct configuration.

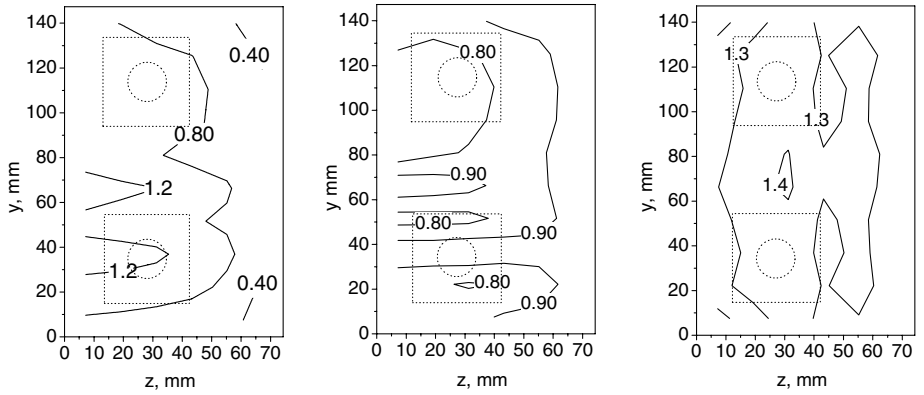

a) Equivalence ratio b) Combustion efficiency c) Mach number

Fig. 4 Properties of combustion gas at the exit of the divergent duct in the case of the 400-mm straight-duct configuration.

B. Short Straight-Duct Configuration

Figure 5 shows the wall pressure distributions at $T_t = 2400$ K, $(O/F)_r = 0.5$, and $\phi = 1.0$ in the case of the 160-mm straight-duct configuration. Under the no-fuel condition, the wall pressure increased from $x = 600$ mm toward the ambient pressure. This showed that the flow was separated around the exit of the model.

Because the wall pressure increased in the divergent-duct section, it is evident that the combustion progressed primarily in the downstream divergent duct. The maximum wall pressure was 1.75 times as high as that of the inflow air. Though the pressure was not high around the exit of the rocket nozzle at $x = 0$, in the divergent duct, it was higher than the ambient pressure of 100 kPa. The thrust was expected to be higher than that with the long straight-duct condition, in which pressure was high in the straight duct and low in the divergent duct.

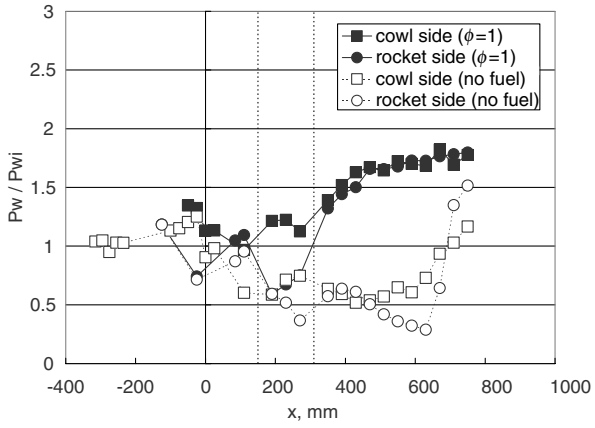

Fig. 5 Wall pressure distribution with 16-mm straight duct.

Figures 6a–6c show the distributions of the local equivalence ratio, the local combustion efficiency, and the Mach number at the exit of the divergent duct, respectively. The equivalence ratios were larger on the rocket side. The combustion efficiencies were distributed around 0.8 to 0.9 on most of the measured plane.

Probing at the exit of the straight duct could not be conducted because of the separation induced by the pitot probes. Mean combustion gas properties at the exit of the divergent duct in the case of the 160-mm straight duct are $\eta_c = 0.74$, $M = 0.99$, and the impulse function is 2548 N.

The combustion gases choked thermally at the exit of the divergent duct. In the case of the short straight-duct configuration, the equivalence ratio and the Mach number showed more distorted distributions than those in the case of the long straight-duct configuration. It is fair to say that the mixing did not progress compared with that in the case of the longer straight duct. Because the wall pressure increased toward the exit, the mean Mach number of the combustion gas should be larger than unity in the divergent duct, but the mean combustion efficiency was lower. The wall pressure around the rocket base, $x = 0$ mm, and the ramp block, $-75 < x < 75$ mm, was not so high. This means that the reaction force in the rocket section was small. The configurations with the shorter straight duct did not produce large thrust.

C. Effect of the Length of the Straight Duct

Figures 7–9 show the wall pressure distributions at $T_t = 2400$ K, $(O/F)_r = 0.5$, and $\phi = 1.0$ in the case of 0, 240, and 320-mm straight-duct configurations, respectively. The 160-mm-length results are presented in Fig. 5. The 400-mm-length case are presented in Fig. 2.

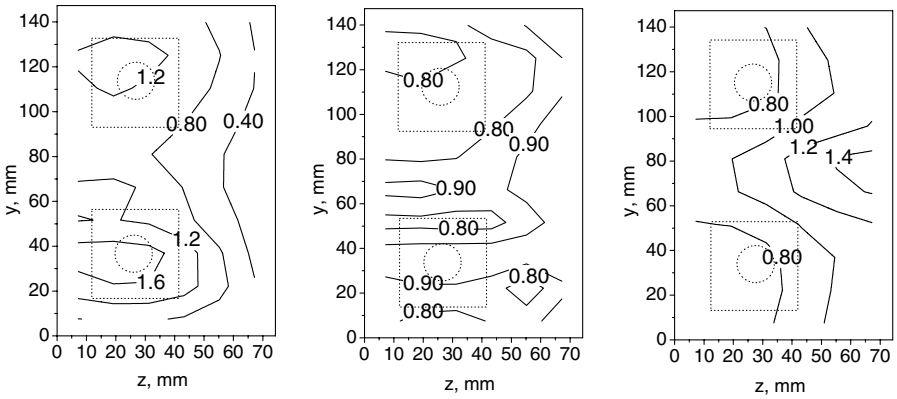

a) Equivalence ratio b) Combustion efficiency c) Mach number

Fig. 6 Properties of combustion gas at the exit of the divergent duct in the case of the 160-mm straight-duct configuration.

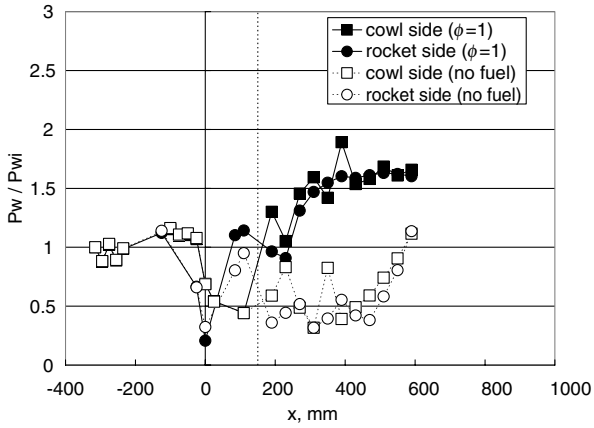

Fig. 7 Wall pressure distribution with 0-mm straight duct.

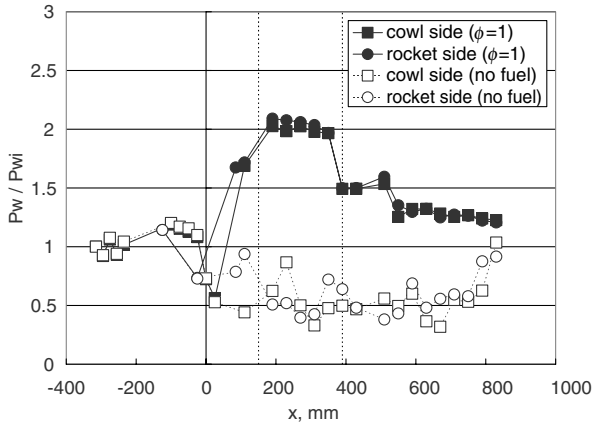

Fig. 8 Wall pressure distribution with 240-mm straight duct.

Depending on the length of the straight duct, two types of combustion patterns were observed. In the cases of the longer straight-duct configurations (240, 320, and 400 mm), the wall pressure increased in the straight-duct section. In the cases of the shorter straight-duct configurations (0 or 160 mm), the wall pressure increased in the divergent duct. The maximum wall pressure was attained in the case of the 400-mm straight-duct configuration: it was 2.5 times higher than that of the inflow air.

The mean combustion efficiencies at the exit of the straight duct and at the exit of the divergent duct are listed in Table 2. This means that the combustion progressed in the straight duct with longer straight-duct configurations and that further reaction occurred in the divergent section.

As previously mentioned, in the case of shorter straight-duct configurations, the equivalence ratio and the Mach number distributions showed nonuniformity, in contrast to those with the longer straight-duct configurations. Mixing did not progress sufficiently, compared with that in the case of the longer straight duct.

These results indicate that the combustion efficiency and the impulse function were higher with longer straight-duct conditions. In the cases of 240-mm ($L/H = 6.3$) and 320-mm ($L/H = 7.6$) straight-duct configurations, the wall pressure patterns and the combustion efficiency at the exit of the divergent duct were almost the same. In the cases of 320-mm ($L/H = 7.6$) and 400-mm ($L/H = 8.9$) straight-duct configurations, the impulse functions

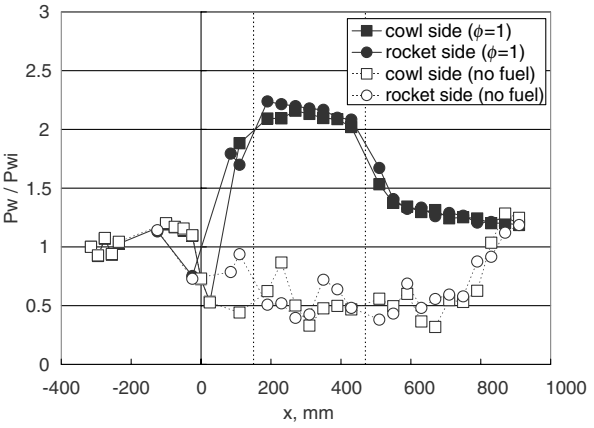

Fig. 9 Wall pressure distribution with 320-mm straight duct.

Table 2 Combustion gas properties

	Exit of straight duct		Exit of divergent duct		
Length of straight duct	Combustion efficiency	Mach number	Combustion efficiency	Mach number	Impulse function
0 mm ($L/H = 2.4$)	——	——	0.66	0.90	2200 N
160 mm ($L/H = 5.0$)	——	——	0.74	0.99	2500 N
240 mm ($L/H = 6.3$)	0.65	0.93	0.78	1.25	2600 N
320 mm ($L/H = 7.6$)	0.68	0.99	0.79	1.30	2700 N
400 mm ($L/H = 8.9$)	0.74	0.79	0.82	1.30	2700 N

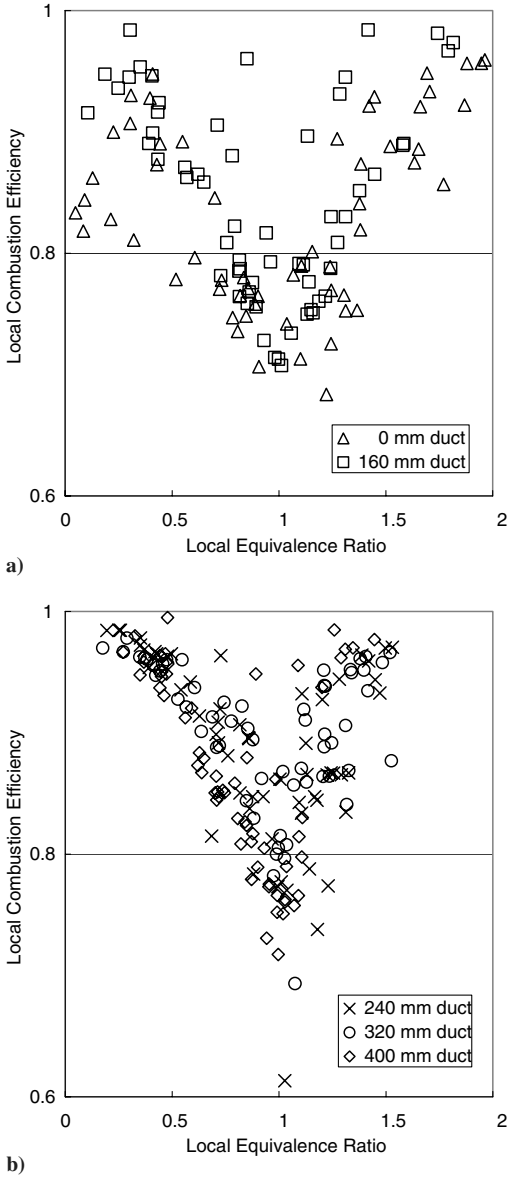

Fig. 10 Correlation between local equivalence ratio and local combustion efficiency in the case of a) shorter duct-combustion efficiency in the case of shorter straight-duct configurations and b) longer straight-duct configurations.

were almost the same. Because the inflow impulse functions were constant for all cases, the thrust performance was defined with the outflow impulse function. The combustion conditions changed at $L/H = 7.5$ and high thrust performance was also attained at $L/H = 7.5$. This was due to the high pressure around the base of the rockets and the ramp channels between the rockets, and between the rockets and the sidewalls.

The combustion conditions with the long straight-duct configurations were greatly different from those with the short straight-duct configurations. The combustion conditions significantly depended on the length of the straight duct. In the cases of the shorter straight-duct configurations, the wall pressure in the divergent-duct section was higher than that of the longer straight-duct configurations. The thrust in the cases of the shorter straight-duct configurations were mainly generated in the divergent duct.

D. Correlation Between Local Equivalence Ratio and Local Combustion Efficiency

Figures 10a and 10b show the correlations of the local equivalence ratio and the local combustion efficiency. In the figures, the local combustion efficiency had a lower value, near $\phi = 1.0$. The excess H_2 when $\phi > 1.0$ and excess O_2 when $\phi < 1.0$ were sampled during the gas-sampling time. They eventually mixed with each other in a sampling bottle, which resulted in lower local combustion efficiency [6]. These results mean that the combustion conditions in these cases were primarily controlled by fuel mixing.

The direction of fuel injection from the rockets was parallel to the supersonic airflow. The mixing efficiency rapidly decreases as Mach number increases to the supersonic regime [7]. The combustion conditions depended on the L/H. In cases of the longer straight-duct configurations, the Mach numbers in the straight duct were subsonic and the mixing efficiencies were higher. This also resulted in higher combustion efficiency.

IV. Conclusions

To demonstrate the operation of the combined-cycle engine under the Mach-8 flight condition, a combustor model was tested at a total temperature of 2400 K and a total pressure of 1.0 MPa. Four kinds of straight duct with various lengths were connected downstream of the rocket section. The results are summarized as follows:

1) Pressure increase due to combustion was attained in the combined-cycle-engine combustor model, in which fuel was injected parallel to the airflow from the rocket nozzles.

2) Combustion efficiency around 0.8 was achieved under the configuration with a longer straight duct downstream of the rocket section. Combustion gas was decelerated to subsonic speed and thermally choked at the exit of the straight duct.

3) The combustion condition with the shorter straight duct was different from that with the longer straight duct. Though a higher level of pressure in the divergent duct was attained, the combustion efficiency and the impulse function were not as high as those with the longer ducts. The combustion conditions in the combustor were greatly changed around $L/H = 7.5$.

4) The combustion conditions at the exit of the divergent duct for all cases were primarily controlled by fuel mixing. In the cases of the longer straight-duct configuration, the Mach numbers in the straight duct were subsonic and the mixing efficiencies were high. This resulted in high combustion efficiency.

References

[1] Hueter, U., and McClinton, C. R., "NASA's Advanced Space Transportation Hypersonic Program," AIAA Paper 2002-5175, Sep. 2002.

[2] Escher, W. J. D., "A, U. S. History of Airbreathing/Rocket Combined-Cycle (RBCC) Propulsion for Powering Future Aerospace Transports, with a Look Ahead to the 2020," International Symposium on Air Breathing Engines Paper 99-7028, Sep. 1999.

[3] Kanda, T., and Kudo, K., "Conceptual Study of a Combined-Cycle Engine for an Aerospace Plane," *Journal of Propulsion and Power*, Vol. 19, No. 5, 2003, pp. 859–867.

[4] Chinzei, N., Komuro, T., Kudo, K., Murakami, A., Tani, K., Masuya, G., and Wakamatsu, Y., "Effects of Injector Geometry on Scramjet Combustor Performance," *Journal of Propulsion and Power*, Vol. 9, No. 1, 1993, pp. 146–152.

[5] Mitani, T., Takahashi, M., Tomioka, S., Hiraiwa, T., and Tani, K., "Analysis and Application of Gas Sampling to Scramjet Engine Testing," *Journal of Propulsion and Power*, Vol. 15, No. 4, 1999, pp. 572–577.

[6] Mitani, T., Chinzei, N., and Kanda, T., "Reaction and Mixing-Controlled Combustion in Scramjet Engines," *Journal of Propulsion and Power*, Vol. 17, No. 2, 1991, pp. 308–314.

[7] John, M., Seiner, S., Dash, M., and Kenzakowski, D. C., "Historical Survey on Enhanced Mixing in Scramjet Engines," *Journal of Propulsion and Power*, Vol. 17, No. 6, 2001, pp. 1273–1286.

R. Bowersox
Associate Editor